Neuron, Vol. 41, 859–865, March 25, 2004, Copyright ©2004 by Cell Press

# A Gating Hinge in $Na^+$ Channels: A Molecular Switch for Electrical Signaling

Report

**Yong Zhao, Vladimir Yarov-Yarovoy, Todd Scheuer, and William A. Catterall***
Department of Pharmacology
Box 357280
University of Washington
Seattle, Washington 98105

## Summary

**Voltage-gated sodium channels are members of a large family with similar pore structures. The mechanism of opening and closing is unknown, but structural studies suggest gating via bending of the inner pore helix at a glycine hinge. Here we provide functional evidence for this gating model for the bacterial sodium channel NaChBac. Mutation of glycine 219 to proline, which would strongly favor bending of the α helix, greatly enhances activation by shifting its voltage dependence −51 mV and slowing deactivation by 2000-fold. The mutation also slows voltage-dependent inactivation by 1200-fold. The effects are specific because substitutions of proline at neighboring positions and substitutions of other amino acids at position 219 have much smaller functional effects. Our results fit a model in which concerted bending at glycine 219 in the S6 segments of NaChBac serves as a gating hinge. This gating motion may be conserved in most members of this large ion channel protein family.**

## Introduction

Voltage-gated sodium channels are responsible for the generation and propagation of action potentials (Hille, 2001; Hodgkin and Huxley, 1952), and mutations in them cause periodic paralysis, arrhythmia, and epilepsy (Keating and Sanguinetti, 2001; Lehmann-Horn and Jurkat-Rott, 1999; Meisler et al., 2002). Sodium channels open and close rapidly in response to changing membrane potential. In eukaryotes, the pore-forming α subunit is composed of four homologous domains containing six transmembrane α helices (S1 to S6) (Catterall, 2000). Electrophysiology, biochemistry, and mutagenesis studies suggest that the S6 transmembrane α helices of each domain form the lining of the inner pore while the linkers between the S5 and S6 segments function as the narrow outer ion selectivity filter. More than 140 related ion channel proteins in mammals share a similar pore structure (Catterall et al., 2002).

The crystal structure of a related bacterial potassium channel (KcsA) with two transmembrane α helices (TM), similar to S5 and S6, in each subunit (Doyle et al., 1998) provides insight into the pore conformation. Functional (Cuello et al., 1998; Heginbotham et al., 1999) and structural (Doyle et al., 1998; Zhou et al., 2001) studies suggest that the crystal structure of KcsA represents the closed state, in which the inner pore-lining helices cross the membrane in an "inverted teepee" conformation to form a closed bundle near the intracellular surface. The crystal structure of a related bacterial calcium-gated potassium channel (MthK) with bound calcium showed that the pore-lining helices are bent about 30° and the helical bundle is splayed open (Jiang et al., 2002a, 2002b). Based on these static crystal structures, it is proposed that these 2-TM potassium channels open by bending the pore-lining helix at a glycine residue at position 83 in MthK (Jiang et al., 2002b). However, functional evidence for this proposal is lacking, and the significance of this proposed gating mechanism for the large family of 6-TM ion channels is unknown.

The overall pore structure of a 6-TM voltage-gated potassium channel is similar to KcsA and MthK (Jiang et al., 2003), and the potential hinge glycine residue is conserved among the 6-TM voltage-gated sodium (Figure 1A), calcium, and potassium channels as well as the cyclic nucleotide-modulated ion channels (Doyle et al., 1998; Durell and Guy, 2001; Flynn and Zagotta, 2001). Here we describe a functional test of the role of this conserved glycine residue (glycine 219; Figure 1A) as a gating hinge in a 6-TM voltage-gated sodium channel from the salt-loving bacterium *Bacillus halodurans* (NaChBac; Ren et al., 2001). Unlike its counterparts in eukaryotes, NaChBac is a homotetramer of separate 6-TM subunits. It activates and inactivates in response to depolarization and selectively conducts sodium, but it resembles both sodium and calcium channels in amino acid sequence and may be an ancestor of both eukaryotic proteins (Ren et al., 2001). Our results show that substitution of a proline for glycine 219, which would strongly favor bending at that position, greatly stabilizes the open state of the channel and dramatically slows its closure. The same mutation also prevents the slow inactivation of NaChBac. Our results provide essential functional support for a gating model in which all four S6 segments undergo a concerted transition to the open state by bending at this hinge glycine and suggest that this gating mechanism is general for 2-TM and most 6-TM ion channels.

## Results

### Enhancement of Activation and Block of Inactivation by a Proline Bend at Position 219 in the S6 Segment

Substitution of a proline residue in an α helix favors bending with a mean angle of 21° to 26° (Barlow and Thornton, 1988; Cordes et al., 2002). In order to mimic the possible open state conformation of G219, we mutated it to proline. The predicted structure of this mutant has the S6 segments bent and splayed open at the intracellular ends (Figures 1B and 1C, magenta), similar to the calcium-activated MthK channel (Jiang et al., 2002a, 2002b). We expressed the G219P mutant in human embryonic kidney tsA-201 cells and analyzed its function by whole-cell voltage clamp. The G219P mutation drastically alters gating properties. NaChBac chan-

*Correspondence: wcatt@u.washington.edu

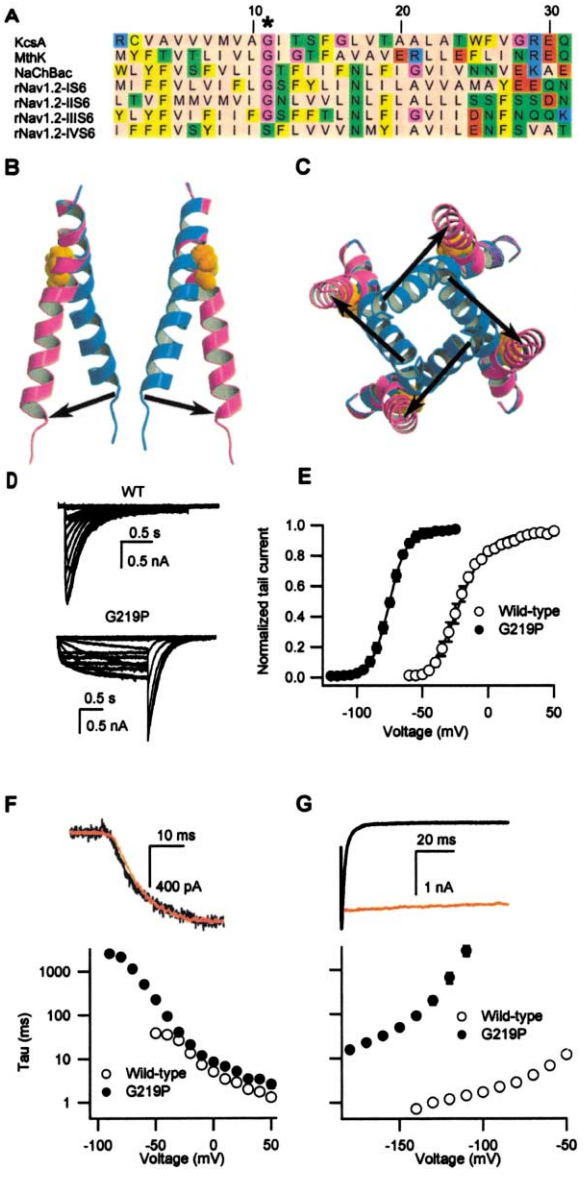


Figure 1. Altered Gating by Substitution of Proline for a Hinge Glycine Residue in the S6 Segment

(A) The conserved glycine in transmembrane helix S6 is labeled by a star in the aligned pore-lining sequences of KcsA, a potassium channel from *Streptomyces lividans*; MthK, a potassium channel from *Methanobacterium thermautotrophicum*; NaChBac, a bacterial sodium channel from *Bacillus halodurans*; and each of the four S6 domains (I–IV) of Nav1.2, a voltage-gated sodium channel from rat brain.

(B and C) Homology model of the proposed change in the preferred position of the S6 segments of NaChBac due to substitution of a proline (in space-filling representation, orange) for glycine (G219P). Model based on Jiang et al. (2002b) as described in Experimental Procedures as the channels move from closed (blue helices) to open (magenta helices) conformations (opening movement shown by arrows). (B) Side view of two channel subunits. (C) View from the cytoplasmic channel surface.

(D) Sodium current records from wt (top) and G219P (bottom) in response to a series of depolarized test-pulse potentials from −55 mV (wt) or −115 mV (G219P) with 10 mV steps from a holding potential of −120 mV.

(E) Voltage dependence of activation from measurements of tail currents after 50 ms (wt) or 2 s (G219P) depolarization. Voltages to activate half of the maximum current ($V_{1/2}$) are −24.0 ± 1.6 mV and −75.2 ± 0.9 mV for wild-type (n = 7) and G219P (n = 7), respectively. The slope factors are 10.8 ± 1.1 mV and 6.8 ± 0.7 mV for wild-type and G219P, respectively.

(F) Sodium current traces during depolarizations to 0 mV (top) and time constants ($\tau$) of activation (bottom) obtained by fitting the final activation phase of currents with single exponentials for wild-type (open circles, n = 6) and G219P (filled circles, n = 6).

(G) Tail currents at −120 mV (top) and time constants of channel closure (bottom) measured during repolarization to the indicated potentials following a test pulse to −10 mV from a holding potential of −120 mV for wild-type (open circles, n = 5) and following a test pulse to −60 mV for G219P (closed circles, n = 8).

nels containing G219P opened at potentials far more negative than wild-type (wt; Figure 1D). The negative gating of NaChBac resulted in a 51 mV negative shift in the voltage dependence of activation (Figure 1E). At strongly negative potentials, G219P channels opened slowly, but activation accelerated with depolarization (Figures 1D and 1F). At potentials where wt NaChBac also opened, the rates of activation of G219P and wt were similar (Figure 1F). In contrast, G219P channels closed extremely slowly upon repolarization, resulting in large, slowly decaying tail currents through channels that remained transiently open upon repolarization to −120 mV (Figure 1G, red). G219P channels did not close at all at potentials more positive than −110 mV, and the rate constant for closure was 2000 times slower than wt at −120 mV (Figure 1G). Evidently, the G219P mutation greatly stabilizes the open state of NaChBac relative to the closed state, as expected from the predicted structural change caused by introduction of proline at position 219 (Figure 1B).

Wild-type NaChBac and G219P channels also display striking differences in inactivation. NaChBac inactivates completely during a 2 s depolarizing pulse (Figures 1D and 2A, top). In contrast, no inactivation is apparent during the test pulses for G219P (Figures 1D and 2A, bottom). This difference in inactivation is reflected in steady-state inactivation curves where wt inactivates completely but no inactivation of G219P is observed during 2 s depolarizing pulses (Figure 2B). Depolarization for 10 min yields approximately 80% inactivation, 1200-fold slower than wt (Figure 2C).

## Positional and Structural Specificity

To examine the positional specificity of these effects, we maintained the native G219 and replaced the adjacent residues isoleucine 218 or threonine 220 with proline (see Figure 1A). These mutations caused comparatively small positive and negative shifts in the voltage dependence of channel activation (Figure 3A, open symbols). Channel closing was slowed 3.3-fold for I218P and 15-fold for T220P (Figure 3B). Both mutations also induced a partial loss of steady-state inactivation (Figure 3C). Each of these effects was significant, but small in comparison to the results of substitution of proline at position 219.

To further probe the function of G219 in NaChBac, we also mutated it to alanine in order to introduce an amino acid that maintains an $\alpha$-helical conformation but is less flexible than glycine. The half-activation voltage

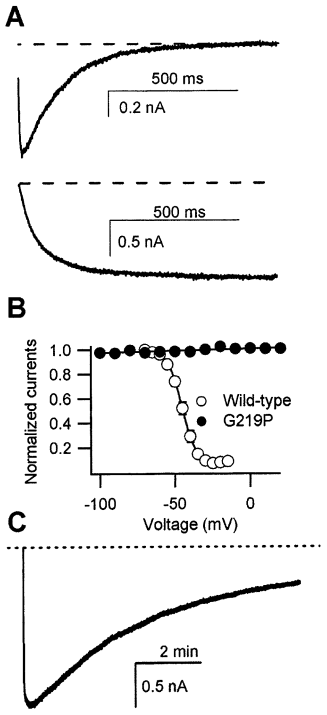


Figure 2. Slowed Inactivation by Substitution of Proline for a Hinge Glycine Residue in the S6 Segment

(A) Representative current traces recorded during test pulses to −10 mV (wt, top) or −60 mV (G219P, bottom) from a holding potential of −120 mV. Dotted lines show zero current level.

(B) Steady-state inactivation was recorded during a test pulse to −10 mV (wt) or −60 mV (G219P) following 2 s long predepolarizations to the indicated potentials (n = 6).

(C) Extremely slow inactivation of G219P during a 10 min long pulse to −60 mV from a holding potential of −120 mV.

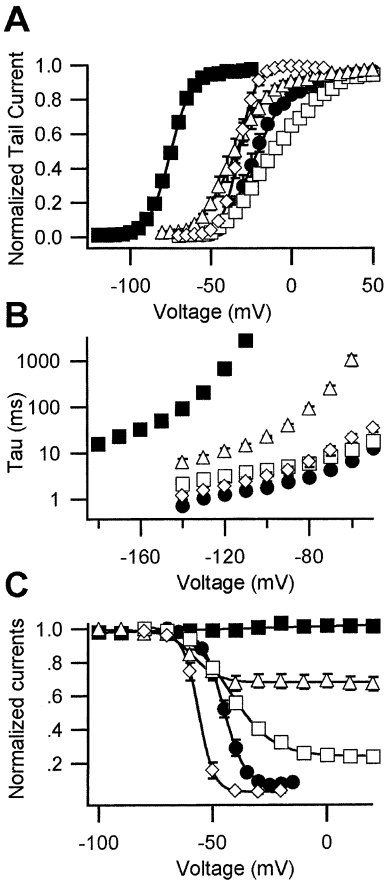


Figure 3. Proline Substitutions Adjacent to G219 and Alanine Substitution for G219 Have Small Effects on Gating

(A) Voltage-dependent activation curves of wt, I218P, T220P, G219A, and G219P channels. The half activation voltages ($V_{1/2}$) were −24.0 ± 1.6 mV, −11.9 ± 2.2 mV, −75.2 ± 0.9 mV, −33.2 ± 1.8 mV, and −35.1 ± 2.9 mV for wt (n = 7), I218P (n = 7), G219P (n = 7), G219A (n = 6), and T220P (n = 7), respectively. The slope factors were 10.8 ± 1.1 mV, 17.0 ± 0.4 mV, 6.8 ± 0.7 mV, 5.8 ± 0.8 mV, and 10.1 ± 1.0 mV. Closed circle, wt; open square, I218P; closed square, G219P; open diamond, G219A; open triangle, T220P.

(B) Time constants of channel closure from single exponential fits to tail currents at different potentials for wt (n = 7), I218P (n = 7), G219P (n = 8), G219A (n = 5), and T220P (n = 7).

(C) Steady-state inactivation curves (Figure 2) from wild-type (n = 6), I218P (n = 4), G219P (n = 6), G219A (n = 6), and T220P (n = 6). Prepulse duration, 2 s. This prepulse duration gives steady-state inactivation for wt and G219A but not for other mutant NaChBac channels.

for G219A was shifted negatively by 9 mV due primarily to a steepening of the activation curve (Figure 3A). Mutation G219A did not change the rate of channel activation, and it slowed channel deactivation only 2-fold in marked contrast to G219P (Figure 3B). Evidently the inflexible, bent conformation favored by proline is necessary for the changes in channel gating observed with the G219P mutant.

### A Concerted Gating Model

How many G219P subunits are required to slow channel closure? The open-state structure of the MthK channel shows that all four inner pore-lining segments are bent (Jiang et al., 2002b). Upon repolarization, channel closure follows a single exponential time course, so a single gating transition is sufficient. If only one NaChBac subunit must straighten its S6 segment for channel closure, a NaChBac channel with only one wt S6 segment should still close rapidly. Because the wt and G219P channels are expressed equally well, expression of a 1:6 ratio of G219P to wt cDNAs is expected to yield primarily a mixture of wt homotetramers, whose functional properties are known, plus heterotetramers with a 1:3 ratio of G219P to wt subunits having altered properties. In contrast to the expectations of an independent gating model, we found that a G219P/wt cDNA ratio of 1:6 yielded heteromultimeric channels with substantially slowed closure (Figure 4A, green). Surprisingly, little or no fast component of tail currents is observed, suggesting that expression of wt homotetramers was suppressed in favor of heterotetramers. This slow closing rate must be due to formation of heterotetrameric channels with a 1:3 ratio of G219P to wt subunits because lower ratios of G219P cDNA did not reveal a different channel type. In contrast, expression of higher ratios of G219P to wt cDNA gave distinct channel species with even slower deactivation rates (data not shown), consistent with formation of oligomers with 2, 3, and eventually 4 G219P subunits.

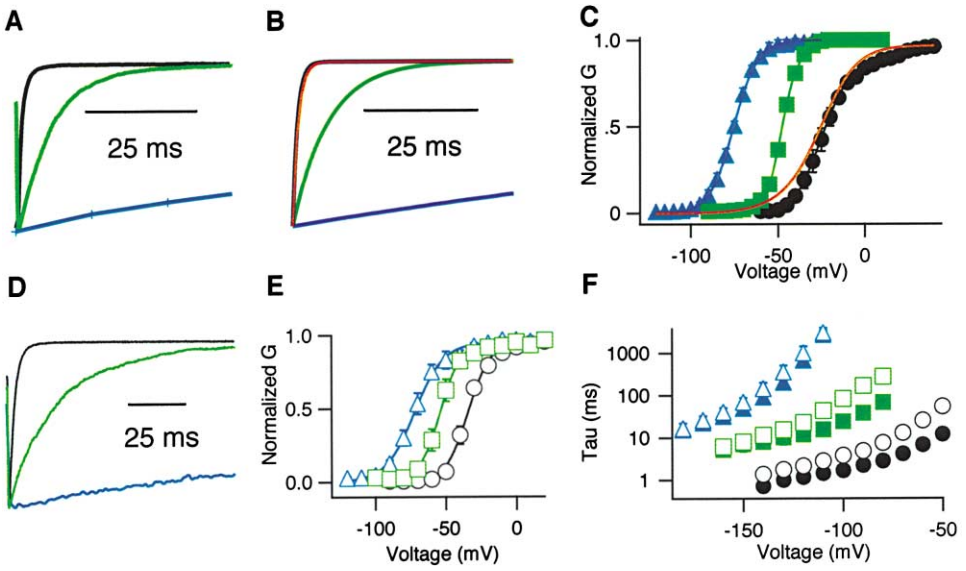


Figure 4. Concerted Gating of Heteromeric Bacterial Sodium Channels

(A) Sodium channel closure for wild-type (black trace), 1:3 G219P:wt (green), and G219P (blue) channels measured as in Figure 1E.

(B) Simulation of the current time courses for the subunit combinations in (A) using a concerted gating model (see text). Red traces are predictions of an independent gating model for 1:3 G219P:wt mixture of subunits; other colors are as in (A).

(C) Activation curves for wt (black circles), 1:3 G219P:wt (green squares), and G219P (blue triangles) channels measured as in Figure 1E. The smooth curves through these points are fits to the model of concerted gating in the text with the values of the rate constant for voltage-independent closure that reproduce the data of (A). The smooth red curve is the prediction, for a 1:3 G219P:wt mixture of subunits, of a gating model in which each of four subunits activates independently and activation of all four subunits is required to produce an open channel (e.g., Hodgkin and Huxley, 1952). For this model, the behavior of the individual subunits was derived from the homomeric wt and G219P subunit channels. For the concerted gating model, voltage-dependent rate constants were calculated as $\alpha = A0\exp(z_\alpha FV/RT)$ and $\beta = B0\exp(-z_\beta V FV/RT)$, where F is Faraday's number, R is the gas constant, T is the absolute temperature, V is the membrane voltage, and $z_\alpha$ and $z_\beta$ are the equivalent charges associated with the $\alpha$ and $\beta$ rate constants, respectively. Initial estimates of the ratios A0/B0, AB, and $\gamma/\delta$, GD, and the voltage dependence of the voltage-dependent transitions were obtained by fitting an equation describing the equilibrium occupancy of the open state of the model (Yifrach and MacKinnon, 2002; Zagotta et al., 1994), $g(V) = (1/g_{max})GD(AB^4)/(1 + AB^4 + (GD^*AB^4)$, to the conductance-voltage curves. For the simulation, $\gamma$ was set at 30,000 because it was poorly defined by the data and the rate of activation was unchanged by the mutations (Figure 1F). The final values obtained from the fitting and simulation procedure were as shown in Supplemental Table S1 (http://www.neuron.org/cgi/content/full/41/6/859/DC1). While these rate constants are not uniquely determined by our data set, the current time courses and voltage dependencies were readily fit by models of this type, whereas fits to the 1:3 G219P:wt subunit mixture were impossible using models requiring mixtures of independently gating subunits. Boltzmann fits to the conductance-voltage relationships used for fitting the model yield values of, for wt, $V_{1/2} = -22.0$ mV, k = 8.9 mV; for G219P:wt, 1:3, $V_{1/2} = -22.0$ mV, k = 6.58 mV; for GP, $V_{1/2} = -75.3$ mV, k = 6.64 mV.

(D) Sodium channel closure from dimeric constructs of wild-type (wt-wt:wt-wt, black trace), 1:1 GP-wt:wt-wt (green), and pure GP-GP:GP-GP (blue).

(E) Activation curves from dimer constructs of wild-type (wt-wt:wt-wt, circles), 1:1 GP-wt:wt-wt (squares), and pure GP-GP:GP-GP (triangles).

(F) Time constants of channel closure for monomer (closed symbols) or dimer (open symbols) constructs of wild-type (circles), 1GP3wt (squares), and 4GP (triangles) measured as in Figure 1G.

To confirm this interpretation of the results, we constructed dimeric NaChBac channels—one with two wt subunits and one with one G219P and one wt subunit. Coexpression of these dimers can give only three products (wt-wt:wt-wt, G219P-wt:wt-wt, and G219P-wt:G219P-wt), and two of these can be unambiguously identified by expression of only the wt dimer or only the mutant G219P-wt dimer. Consistent with our interpretation, we obtained comparable results with these defined heteromers formed from dimers (Figures 4D–4F) as with the mixture of heteromers formed at a 1:6 ratio of wt and G219P monomers (Figures 4A and 4B) when the rate constants for dimers were scaled 2-fold. The wt dimer (wt-wt) expressed alone gave fast deactivation (Figure 4D, black) compared to the dimer with two G219P mutations (G219P-G219P; Figure 4D, blue). The 1:1 mixture of the wt-wt and G219P-wt dimers gave an intermediate rate of deactivation (Figure 4D, green), comparable to the rate of deactivation of the 1:3 ratio of G219P:wt monomers after scaling (Figure 4B, green). In contrast, the dimer with a single G219P mutation expressed alone (G219P-wt:G219P-wt) yielded channels with clearly distinct properties from the 1:1 mixture, including substantially slower rates of deactivation and inactivation (data not shown). Evidently, the deactivation time course of channels formed by the 1:1 mixture of G219P-wt and wt-wt dimers primarily reflects the properties of the wt-wt:G219P-wt heterodimer of dimers because we detect no rapid component of deactivation characteristic of wt and little or no slow component of deactivation or inactivation characteristic of G219P-wt:G219P-wt homodimer of dimers. These striking changes in deactivation rates caused by substitution of a single G219P subunit in heterotetramers formed from either monomers or dimers indicate that one mutant subunit is sufficient to substantially slow closure of the

channel. Evidently, a concerted conformational change resulting from hinge motion at G219 in multiple subunits is needed for channel closure.

In light of these results, it is likely that opening of the channel is also a concerted movement of the four subunits. A simple kinetic model for channel activation by a concerted transition of the four subunits (Smith-Maxwell et al., 1998; Zagotta et al., 1994) includes the following gating transitions:

$$C_4 \underset{\beta}{\overset{4\alpha}{\rightleftharpoons}} C_3 \underset{2\beta}{\overset{3\alpha}{\rightleftharpoons}} C_2 \underset{3\beta}{\overset{2\alpha}{\rightleftharpoons}} C_1 \underset{4\beta}{\overset{\alpha}{\rightleftharpoons}} C_0 \underset{\delta}{\overset{\gamma}{\Leftrightarrow}} O$$

in which $C_X$ denotes a channel state with X subunits in the resting state, O denotes the open state, the paired single-headed arrows denote reversible voltage-dependent transitions of single subunits to their activated state, and the double-headed arrow denotes a voltage-independent, concerted transition of all four subunits to the open state. In this model, each of the four subunits is activated by outward movement of its S4 voltage-sensing segment, driven by depolarization. This is followed by a voltage-independent concerted transition of all four S6 segments into the open conformation. We compared the voltage dependence of activation of NaChBac channels with different ratios of G219P and wt subunits to the predictions of this kinetic model and a fully independent gating model in which the opening transition of each subunit proceeds separately (Figure 4). We found that the fully independent model predicted little change in the rate of deactivation (Figure 4B, red) and much smaller negative shifts in the voltage dependence of activation for a heteromer containing a single G219P subunit than we observed (Figure 4C, red). In contrast, the concerted gating model closely fits our results for G219P when the rate constants for voltage-independent channel closure and voltage-dependent channel deactivation were slowed by 212-fold and 2.5-fold from wt values, respectively (Figure 4B, green). Moreover, the voltage dependence of activation of the 1:3 G219P/wt channel was also accurately fit using rate constants derived from the data of Figure 4A. (Figure 4C, green). Together with our data on slowed closure of channels with a single G219P subunit, these results point to a concerted gating transition involving a hinge-bending motion at G219 as an essential conformational transition opening and closing the pore of NaChBac.

## Discussion

### Glycine 219 as a Molecular Hinge

Our results provide strong functional support for the hypothesis that G219 acts as a hinge point in the S6 segment. Glycine confers flexibility in protein structures (Chakrabartty et al., 1991), while proline confers a bent conformation and structural rigidity imposed by its inability to form intermolecular hydrogen bonds and its cyclic pyrrolidine side chain (Hurley et al., 1992; Williams and Deber, 1991). A proline in an $\alpha$ helix favors bending, with an average angle of 21° to 26° (Barlow and Thornton, 1988; Cordes et al., 2002). Therefore, replacing the glycine hinge at position 219 with a proline is predicted to stabilize a conformation having a bend of 21° to 26°. This conformation is similar to the open state of MthK, as illustrated by the molecular model in Figure 1B. It is evident from this comparison that substitution of proline in this position in NaChBac mimics the conformation of the calcium-liganded MthK channel, providing a clear rationale for stabilization of the open state relative to the closed state by this amino acid substitution. Moreover, the rigidity of the proline in this position resists straightening of the S6 $\alpha$ helix, so the mutant channel closes very slowly and activation is shifted dramatically to more negative membrane potentials by destabilization of the closed state relative to the open state. The close fit between our results and the predictions for proline substitution at a glycine hinge indicate that hinge movements at G219 are indeed an essential determinant of opening and closing of NaChBac channels.

### A Concerted Gating Bend at Glycine 219

The symmetric homotetrameric structure of NaChBac allows a novel test of concerted sodium channel gating by single amino acid substitutions in one subunit of a tetrameric channel. Consistent with a concerted gating model, we find that substitution of a single NaChBac subunit in a homotetramer or in a dimer of dimers causes a marked slowing of channel closure and a marked negative shift in the voltage dependence of activation, which are not predicted by independent gating models. Evidently, NaChBac is gated by concerted bending of all four S6 segments at G219.

### A General Gating Mechanism for the Voltage-Gated Ion Channel Family?

How general is this hinge mechanism of gating for the members of the voltage-gated ion channel family? NaChBac is a probable ancestor of both vertebrate sodium and calcium channels, and the amino acid sequence of its S6 segment is strikingly similar to those of vertebrate sodium channels, ranging up to 60% identity with segment IIIS6 of Nav1.2 channels (Figure 1A). Therefore, it is highly likely that sodium and calcium channels gate via this mechanism. The equivalent of G219 in NaChBac is conserved in 2-TM potassium channels; 6-TM voltage-gated sodium, calcium, and potassium channels; and 6-TM cyclic nucleotide-gated channels and HCN channels, which total 111 family members in the human genome (Catterall et al., 2002). Structural studies support this gating mechanism for 2-TM potassium channels (Jiang et al., 2002a, 2002b), and extensive analyses of site-directed mutants suggest an inner pore helix bending mechanism for 2-TM and 6-TM potassium channels (Jin et al., 2002; Yifrach and MacKinnon, 2002). We suggest that a bending motion at the equivalent of G219 is a crucial element of rapid opening and closing of the pores of this diverse array of ion channels. In contrast, the structurally related 6-TM TRP channels, which activate slowly in response to thermal stimuli or binding of ligands (Clapham et al., 2003), do not have a conserved glycine residue in their S6 segments and may gate slowly because their S6 segments are comparatively inflexible. Similarly, two novel, recently described bacterial sodium channels (Koishi et al., 2003) lack the equivalent of G219. Our results predict that substitutions of glycine in these channels should favor the closed

state and accelerate deactivation, while substitution of proline should favor the open state and slow deactivation. Evidently, the glycine hinge gating mechanism of NaChBac and bacterial potassium channels has been continued as the diverse array of vertebrate ion channels of these families has evolved to serve many different functions in electrical signaling and cellular regulation in the nervous system and elsewhere.

## Experimental Procedures

### Cloning and Site-Directed Mutagenesis

NaChBac cDNA was cloned from *Bacillus halodurans* genomic DNA (American Type Culture Collection, Manassas, VA) by polymerase chain reaction (PCR) using Pfu DNA polymerase (Stratagene, La Jolla, CA) and primers designed according to the deposited sequence (Ren et al., 2001) into pCDM8 vector (Invitrogen, Carlsbad, CA). Site-directed mutagenesis was done based on PCR of the full-length plasmid pCDM8 containing NaChBac cDNA using high-fidelity Pfu DNA polymerase (method by Stratagene) and verified by sequencing. cDNA encoding a dimer was constructed by ligating two NaChBac cDNAs at a Pst I restriction site with a 12-Gly linker in between. The stop codon in the first NaChBac domain was removed. The amino acid residues that were inserted between the two domains are GGGGGGLQGGGGGG.

### Transient Expression of NaChBac in tsA-201 Cells

Human embryonic kidney tsA-201 cells, a simian virus (SV40) large T antigen-expressing derivative of HEK-293 cells (Robert Dubridge, Cell Genesis, Foster City, CA), were maintained in Dulbecco's modified Eagle medium/F12 medium (Invitrogen) supplemented with 10% fetal bovine serum (Hyclone, Logan, UT), 25 units of penicillin per ml, and 25 μg of streptomycin per ml (Sigma). Cells were cotransfected with either wild-type or mutant NaChBac constructs and a vector encoding the human CD8 cell surface protein (EBO-pCD-leu2; American Type Culture Collection) as described (Margolskee et al., 1993). Transiently transfected cells were visualized with magnetic polystyrene microspheres precoated with anti-CD8 antibody (Dynabeads M-450 CD8, Dynal, Great Neck, NY) (Jurman et al., 1994).

### Electrophysiological Recording

Whole-cell voltage-clamp experiments were performed on transiently transfected tsA-201 cells at 22°C as described previously (Qu et al., 1995) using an extracellular solution containing (in mM) NaCl (140), $CaCl_2$ (2), $MgCl_2$ (2), HEPES (10) (pH 7.4), and an intracellular (pipette) solution containing (in mM) N-methyl-D-glucamine (NMG 179), EGTA (10), NaCl (8), $MgCl_2$ (4), HEPES (40) (pH 7.5). Electrodes were formed from glass micropipettes (VWR, West Chester, PA), and currents were recorded with an Axopatch 200B amplifier (Axon Instruments, Union City, CA). Cell and electrode capacitance and series resistance were compensated with internal voltage-clamp circuitry. Residual linear leak and capacitance were subtracted by using a P/4 protocol. Pulses were generated and data were collected with ITC-18 computer interface (Instrutech Corporation, Port Washington, NY) and Pulse 8.0 software (HEKA, Germany). Data were analyzed by Igor Pro 4.00 (Wavemetrics, Lake Oswego, OR). Half activation and inactivation voltages were derived from fits of a Boltzmann function, $1/(1 + \exp((V - V_{1/2})/k)$ to voltage-dependent activation curves from normalized tail currents, or to steady-state inactivation curves, respectively, where k was a slope factor. Time constants of activation and deactivation were obtained by fitting the activation currents or deactivation currents (tail currents) with a single exponential. Results are reported as mean ± SEM.

Simulations of currents by models were carried out using the Runge-Kutta method implemented in a custom-written program in Igor Pro. To obtain initial estimates of equilibrium constants, an equation describing the equilibrium voltage dependence of the open state (Smith-Maxwell et al., 1998; Yifrach and MacKinnon, 2002; Zagotta et al., 1994) was fit to the experimentally derived conductance-voltage relationships for the wt and mutant constructs by a least-squares approach. Current time courses at different activation voltages and tail currents at −120 mV were simulated, preserving these ratios of equilibrium constants.

### Multiple Sequence Alignment and Homology Modeling

Sequence alignment between M2 segment of KcsA, M2 segment of MthK, S6 segment of NaChBac, and S6 segments from all four domains of $rNa_v1.2$ was performed using ClustalX software (Jeanmougin et al., 1998) and then manually adjusted to specifically align glycine residues in the middle of M2 segment of KcsA and S6 segment of NaChBac. Residues were colored with Jalview (http://www.ebi.ac.uk/~michele/jalview) using the Zappo color scheme, where hydrophobic residues (I, L, V, A, and M) are colored pink, aromatic residues (F, W, and Y) are colored orange, positively charged residues (K, R, and H) are colored blue, negatively charged residues (D and E) are colored red, hydrophilic residues (S, T, N, and Q) are colored green, P and G are colored magenta, and C is colored yellow.

Homology modeling and proline bend simulation were performed using Molecular Operating Environment software (Chemical Computing Group, Inc.) and illustrated with MOLSCRIPT (Kraulis, 1991) and RASTER-3D (Merritt and Bacon, 1997). The KcsA channel structure (Doyle et al., 1998) was used as a primary template. Proline bends in the central section of 50 transmembrane α helices have an average bend angle of 21° ± 11° (Cordes et al., 2002). We extracted this data set using the Molecular Operating Environment software (Chemical Computing Group, Inc.) and the Prokink protocol (Visiers et al., 2000) of the Simulaid program (Mezei, 1997; http://fulcrum.physbio.mssm.edu/~mezei/simulaid). This analysis yielded average proline kink angle of 19° ± 12° (data not shown) in close agreement with average proline kink reported by Cordes et al. (2002). The proline swivel angle varied widely in this data set (−17° ± 120°), indicating little energetic difference across a wide range of swivel angles. We used the swivel angle of the proline bend in the glycerol transporter (Fu et al., 2000) (PDB code 1FX8) as a model for NaChBac.

## Acknowledgments

This research was supported by NIH Research Grants R01 NS15751 to W.A.C. and K01 MH67625 to V.Y.-Y.

Received: December 18, 2003
Revised: January 23, 2004
Accepted: January 26, 2004
Published: March 24, 2004

## References

Barlow, D.J., and Thornton, J.M. (1988). Helix geometry in proteins. J. Mol. Biol. *201*, 601–619.

Catterall, W.A. (2000). From ionic currents to molecular mechanisms: the structure and function of voltage-gated sodium channels. Neuron *26*, 13–25.

Catterall, W.A., Chandy, K.G., and Gutman, G.A., eds. (2002). The IUPHAR Compendium of Voltage-Gated Ion Channels (Leeds, UK: IUPHAR Media).

Chakrabartty, A., Schellman, J.A., and Baldwin, R.L. (1991). Large differences in the helix propensities of alanine and glycine. Nature *351*, 586–588.

Clapham, D.E., Montell, C., Schultz, G., and Julius, D. (2003). International union of pharmacology. XLIII. Compendium of voltage-gated ion channels: transient receptor potential channels. Pharmacol. Rev. *55*, 591–596.

Cordes, F.S., Bright, J.N., and Sansom, M.S. (2002). Proline-induced distortions of transmembrane helices. J. Mol. Biol. *323*, 951–960.

Cuello, L.G., Romero, J.G., Cortes, D.M., and Perozo, E. (1998). pH-dependent gating in the *Streptomyces lividans* $K^+$ channel. Biochemistry *37*, 3229–3236.

Doyle, D.A., Morais Cabral, J., Pfuetzner, R.A., Kuo, A., Gulbis, J.M., Cohen, S.L., Chait, B.T., and MacKinnon, R. (1998). The structure of the potassium channel: molecular basis of $K^+$ conduction and selectivity. Science *280*, 69–77.

Durell, S.R., and Guy, H.R. (2001). A family of putative Kir potassium channels in prokaryotes. BMC Evol. Biol. *1*, 14.

Flynn, G.E., and Zagotta, W.N. (2001). Conformational changes in S6 coupled to the opening of cyclic nucleotide-gated channels. Neuron *30*, 689–698.

Fu, D., Libson, A., Miercke, L.J., Weitzman, C., Nollert, P., Krucinski, J., and Stroud, R.M. (2000). Structure of a glycerol-conducting channel and the basis for its selectivity. Science *290*, 481–486.

Heginbotham, L., LeMasurier, M., Kolmakova-Partensky, L., and Miller, C. (1999). Single *Streptomyces lividans* $K^+$ channels: functional asymmetries and sidedness of proton activation. J. Gen. Physiol. *114*, 551–560.

Hille, B. (2001). Ion Channels of Excitable Membranes, third edition (Sunderland, MA: Sinauer Associates).

Hodgkin, A.L., and Huxley, A.F. (1952). A quantitative description of membrane current and its application to conduction and excitation in nerve. J. Physiol. *117*, 500–544.

Hurley, J.H., Mason, D.A., and Matthews, B.W. (1992). Flexible-geometry conformational energy maps for the amino acid residue preceding a proline. Biopolymers *32*, 1443–1446.

Jeanmougin, F., Thompson, J.D., Gouy, M., Higgins, D.G., and Gibson, T.J. (1998). Multiple sequence alignment with Clustal X. Trends Biochem. Sci. *23*, 403–405.

Jiang, Y., Lee, A., Chen, J., Cadene, M., Chait, B.T., and MacKinnon, R. (2002a). Crystal structure and mechanism of a calcium-gated potassium channel. Nature *417*, 515–522.

Jiang, Y., Lee, A., Chen, J., Cadene, M., Chait, B.T., and MacKinnon, R. (2002b). The open pore conformation of potassium channels. Nature *417*, 523–526.

Jiang, Y., Lee, A., Chen, J., Ruta, V., Cadene, M., Chait, B.T., and MacKinnon, R. (2003). X-ray structure of a voltage-dependent $K^+$ channel. Nature *423*, 33–41.

Jin, T., Peng, L., Mirshahi, T., Rohacs, T., Chan, K.W., Sanchez, R., and Logothetis, D.E. (2002). The $\beta\gamma$ subunits of G proteins gate a $K^+$ channel by pivoted bending of a transmembrane segment. Mol. Cell *10*, 469–481.

Jurman, M.E., Boland, L.M., Liu, Y., and Yellen, G. (1994). Visual identification of individual transfected cells for electrophysiology using antibody-coated beads. Biotechniques *17*, 876–881.

Keating, M.T., and Sanguinetti, M.C. (2001). Molecular and cellular mechanisms of cardiac arrhythmias. Cell *104*, 569–580.

Koishi, R., Xu, H., Ren, D., Navarro, B., Spiller, B.W., Shi, Q., and Clapham, D.E. (2003). A superfamily of voltage-gated sodium channels in bacteria. J. Biol. Chem., in press. Published online December 9, 2003. 10.1074/jbc.M313100200.

Kraulis, P.J. (1991). MOLSCRIPT: a program to produce both detailed and schematic plots of protein structures. J. Appl. Crystallogr. *24*, 946–950.

Lehmann-Horn, F., and Jurkat-Rott, K. (1999). Voltage-gated ion channels and hereditary disease. Physiol. Rev. *79*, 1317–1372.

Margolskee, R.F., McHendry-Rinde, B., and Horn, R. (1993). Panning transfected cells for electrophysiological studies. Biotechniques *15*, 906–911.

Meisler, M.H., Kearney, J.A., Sprunger, L.K., MacDonald, B.T., Buchner, D.A., and Escayg, A. (2002). Mutations of voltage-gated sodium channels in movement disorders and epilepsy. Novartis Found. Symp. *241*, 72–86, 226–232.

Merritt, E.A., and Bacon, D.J. (1997). Raster3D photorealistic molecular graphics. Methods Enzymol. *277*, 505–524.

Mezei, M. (1997). Optimal position of the solute for simulations. J. Comp. Chem. *18*, 812–815.

Qu, Y., Rogers, J., Tanada, T., Scheuer, T., and Catterall, W.A. (1995). Molecular determinants of drug access to the receptor site for antiarrhythmic drugs in the cardiac $Na^+$ channel. Proc. Natl. Acad. Sci. USA *92*, 11839–11843.

Ren, D., Navarro, B., Xu, H., Yue, L., Shi, Q., and Clapham, D.E. (2001). A prokaryotic voltage-gated sodium channel. Science *294*, 2372–2375.

Smith-Maxwell, C.J., Ledwell, J.L., and Aldrich, R.W. (1998). Role of the S4 segment in cooperativity of voltage-dependent potassium channel activation. J. Gen. Physiol. *111*, 399–420.

Visiers, I., Braunheim, B.B., and Weinstein, H. (2000). Prokink: a protocol for numerical evaluation of helix distortions by proline. Protein Eng. *13*, 603–606.

Williams, K.A., and Deber, C.M. (1991). Proline residues in transmembrane helices: structural or dynamic role? Biochemistry *30*, 8919–8923.

Yifrach, O., and MacKinnon, R. (2002). Energetics of pore opening in a voltage-gated $K^+$ channel. Cell *111*, 231–239.

Zagotta, W.N., Hoshi, T., and Aldrich, R.W. (1994). Shaker potassium channel gating. III: Evaluation of kinetic models for activation. J. Gen. Physiol. *103*, 321–362.

Zhou, Y., Morais-Cabral, J.H., Kaufman, A., and MacKinnon, R. (2001). Chemistry of ion coordination and hydration revealed by a $K^+$ channel-Fab complex at 2.0 Å resolution. Nature *414*, 43–48.